Macromolecules

pubs.acs.org/Macromolecules Article

High-Throughput FRAP Analysis of Solute Diffusion in Hydrogels

Nathan R. Richbourg and Nicholas A. Peppas*

Cite This: *Macromolecules* 2021, 54, 10477−10486 Read Online

ACCESS | Metrics & More | Article Recommendations | Supporting Information

ABSTRACT: Increasingly accurate mathematical models have been developed to relate solute and hydrogel properties to solute diffusion coefficients in hydrogels, primarily by comparing solute sizes and hydrogel mesh sizes. Here, we use a standardized, high-throughput method for fluorescence recovery after photobleaching (FRAP) experiments and analysis to characterize the diffusion coefficients of fluorescein, three sizes of FITC-dextran, and three sizes of FITC-conjugated poly(ethylene glycol) (PEG) through 18 structurally varied poly(vinyl alcohol) (PVA) hydrogel formulations. Increasing the hydrogel mesh radii increased the diffusivities of all the tested solutes within the hydrogels. While the diffusivity of FITC-dextrans in hydrogels decreased with increasing solute size, the diffusivity of FITC-PEGs increased with increasing solute size, suggesting that a generalized hydrodynamic radius-based model is not universally applicable for solute diffusion in hydrogels. The high-throughput characterization method for solute diffusion in hydrogels described here facilitates precise hydrogel design for biomedical applications.

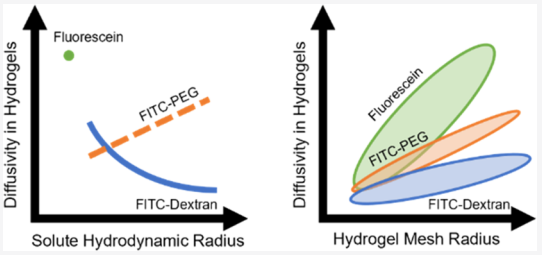

INTRODUCTION

In biological and biomedical applications, including drug release devices and extracellular matrix-mimicking cell culture scaffolds, hydrogels are used as reservoirs for water-soluble, environmentally sensitive molecules such as antibodies, cytokines, and siRNA.[1−4] Because the polymer network component of hydrogels interrupts internal convection, diffusive transport often controls solute movement within and release from hydrogels. Therefore, solute diffusivity in hydrogels is critical to the design of hydrogel-based tissue engineering scaffolds and drug delivery devices.

Solute properties greatly influence how it diffuses in a hydrogel. Studies of solute diffusivity in hydrogels have utilized well-characterized solutes such as very often commercially available fluorescein isothiocyanate-conjugated dextran (FITC-dextran) molecules.[5−13] FITC-dextrans are water-soluble fluorescent molecules with controllable size distributions based on the molecular weight of the dextran component. According to the Stokes−Einstein theory, increasing the solute size reduces diffusivity in free solution. Within hydrogels, the relationship between solute diffusivity and solute size is further complicated by the concentration of polymer in the hydrogel and the size of portals created by the network structure.[14,15] FITC-dextrans with molecular weights at 4, 10, and 20 kDa have been frequently used to study solute diffusivity in hydrogels because they are similar in size to hydrogel network portals and cytokines.[6−10] Beyond FITC-dextrans, fluorescein, FITC-conjugated bovine serum albumin, and other molecules have been used as smaller, larger, protein-representative, shape-varied, and chemically interacting solutes diffusing in hydrogels.[6,7,16,17] Given the potential for shape-based and chemical interactions between solutes and a polymer network, it is unclear whether the solute diffusivity profiles of FITC-dextrans in hydrogels correspond to equivalently sized biomacromolecules.

As with solutes, analysis of how hydrogel properties affect solute diffusivity in hydrogels has focused on the relative sizes of molecular components.[6,10,13,16,18] Mesh size, which describes the average distance between two network junctions connected by a polymer chain,[19] has been frequently associated with solute diffusivities in hydrogels via convenient, often simplified, correlations or scaling concepts. We recently suggested that the term "mesh radius," which describes the expected radius of a hydrodynamically spherical solute that would pass through a hydrogel network portal, would be a more accurate predictor of solute diffusivity than mesh size.[15] Both mesh size and mesh radius can be predicted via the swollen polymer network model[20] and can be further applied through the multiscale diffusion model[14] to estimate solute diffusivity within hydrogels.

Fluorescence recovery after photobleaching (FRAP) experiments are a fast and efficient method for characterizing solute diffusivity within hydrogels.[21−23] FRAP experiments briefly photobleach fluorescent solutes using a high-powered laser and then repeatedly capture fluorescence micrographs of the

Received: August 19, 2021
Revised: October 13, 2021
Published: November 9, 2021

https://doi.org/10.1021/acs.macromol.1c01752
Macromolecules 2021, 54, 10477−10486

bleached spot and surrounding area as nearby solutes that retain their fluorescence diffuse into the bleached spot. Unlike traditional incubation and release experiments, FRAP experiments are conducted at steady state (bleached solutes remain otherwise identical to unbleached solutes) within the bulk of a hydrogel, minimizing experimental and modeling errors associated with solute concentration gradients and partitioning at the interface of the hydrogel and the bulk solution.[6,24] FRAP experiments performed using confocal laser scanning microscopes provide data with exceptionally high spatial and temporal resolutions, and programs that comprehensively interpret these datasets provide increasingly accurate and precise calculations of solute diffusion coefficients.[21,25−27] These recent and ongoing technological developments associated with FRAP experiments make FRAP a promising tool for high-throughput characterization of solute diffusivities in hydrogels.

The great variety of solutes and hydrogel formulations studied for diffusional biomedical applications warrants high-throughput analysis methods to create a robust perspective of solute diffusion in hydrogels, inform fundamental models, and improve hydrogel design for biomedical applications. Here, we modified the highly accurate FRAP analysis program of Jönsson et al.[27] for high-throughput analysis of standardized FRAP experiments in hydrogels. Using the new modified program, we analyzed 7 solutes diffusing in 18 hydrogel formulations. We compared the size- and chemistry-dependent diffusion of FITC-dextrans with FITC-conjugated poly(ethylene glycol) molecules (FITC-PEGs) and fluorescein. Poly(vinyl alcohol) (PVA) hydrogels were synthesized with varying initial polymer volume fractions and degrees of polymerization between junctions, two structural parameters that independently affect mesh radius and solute diffusivity within the synthesized hydrogels. The resulting coordinated analysis tested assumptions and practical limitations of existing models for solute diffusion in hydrogels, suggesting a path toward more comprehensive and effective modeling and hydrogel design.

METHODS

PVA Hydrogel Synthesis and Swelling Characterization. Poly(vinyl alcohol) (PVA) hydrogels were synthesized as previously described.[28] Briefly, well-characterized PVA (Sigma-Aldrich, St. Louis, MO) was dissolved in deionized water by heating at 90 °C overnight at three concentrations corresponding to three initial polymer volume fractions (φ_0) of 5, 7.5, and 10%. An aqueous glutaraldehyde solution (25%; Sigma-Aldrich) was added based on stoichiometric ratios with PVA (mol glutaraldehyde/mol PVA-repeating units) to attain six ideal degrees of polymerization between junctions (N_j) of 20, 30, 40, 50, 60, and 70. The resulting 18 combinations of initial polymer volume fraction and degree of polymerization values were cast on 2 mm thick sheets and left to react for 3 h to form hydrogels. Following the hydrogel formation reaction, three 18 mm diameter discs were punched for swelling analysis, and the remaining material was swollen in phosphate-buffered saline (PBS) for use in fluorescence recovery after photobleaching (FRAP) experiments. All hydrogel formulations were synthesized twice to demonstrate batch-to-batch reproducibility. The formulation with the greatest concentration of polymer and junctions ($\varphi_0 = 0.100$, $N_j = 20$) only formed intact hydrogels in one of the batches.

As previously described,[28] swelling was characterized in three states: The relaxed state immediately followed gelation, the swollen state followed swelling to equilibrium in excess PBS, and the dry state followed desalting in deionized water and drying with heat and vacuum. Volumes in each state were measured using a buoyancy-based method. Swollen polymer volume fractions (φ_s) were calculated by dividing the swollen volume by the dry volume. The mesh radius (r_m) of each formulation was calculated based on swollen polymer volume fractions and hydrogel structural parameters (eq 1).[15] Eq 1 only applies to swollen polymer networks with tetrafunctional junctions.

$$r_m = \frac{\sqrt{6}}{3}\varphi_s^{-1/3}\left[\left(1 - \frac{2}{f}\right)\bar{l}^2 C_\infty \lambda N_j\right]^{1/2} \quad (1)$$

In eq 1, f is the network junction functionality (4 for glutaraldehyde-crosslinked PVA), $\bar{l}$ is the weighted average of the bond lengths in the backbone of the repeating unit (for PVA, 0.154 nm), C_∞ is the Flory characteristic ratio (for PVA, 8.3), and λ is the number of linear backbone bonds per repeating unit (for PVA, 2).[28]

FRAP Experiments. Fluorescein (Sigma-Aldrich), three sizes of FITC-dextran (Sigma-Aldrich), and three sizes of FITC-PEGs (Creative PEGWorks, Durham, NC) were selected as solutes to study diffusivity within hydrogels via FRAP experiments with a confocal microscope (Zeiss LSM710 Confocal Microscope, Germany). Solute diffusion experiments in aqueous solution with 10 μM mL^{-1} of each solute in PBS and solute diffusion experiments in hydrogels were prepared by incubating swollen hydrogel punches (5 mm diameter, ∼2 mm height, three punches per hydrogel formulation and batch) in 5 mL of 10 μM mL^{-1} solute-loaded solution in black 5 mL centrifuge tubes overnight with orbital shaking. All FRAP experiments were performed using eight-chambered microscope slides with no. 1.5 glass bottoms (Cellvis, Mountain View, CA), 2× zoom on a 20× objective lens (NA = 0.80, WD = 0.55 mm), 512 × 512 pixel images, a 128-pixel bleach spot diameter (∼54 μm), and 60 frames taken at the fastest scan rate available (∼240 ms per frame, with 0.3 s total delay between frames). Imaging and bleaching were performed using a 405 nm argon laser at 100% intensity for bleaching and 2−20% power and 600−900 gain as needed for the recovery imaging. For all samples, three scans at different locations within the sample were taken, all at a depth of 100 μm into the sample.[8] The FRAP experiment protocol, experimental data, and experimental parameters are available in the Supporting Information.

FRAP Experiment Analysis and Modeling. Raw image sequence files from the confocal microscope were preprocessed for analysis. Specifically, Carl Zeiss image files (.czi) were converted to tagged image format files (.tif) using ImageJ with the Bio-Formats Macro Extensions plugin. Experimental data were then individually analyzed as discussed below to calculate diffusion coefficients and immobilized solute fractions using the Jönsson et al. FRAP analysis program[27] in MATLAB R2018b (MathWorks, Natick, MA). Experimental data were also analyzed using a novel modification of the FRAP analysis program optimized for high-throughput batch analysis. The novel FRAP analysis program is available in the Supporting Information.

Following the calculation of diffusion coefficients, further analysis and regrouping of the data were performed using R and RStudio (RStudio, Boston, MA). FRAP experiment data were summarized and grouped according to solute-formulation pairings. Literature-based estimates of the solute diffusivities in solution were calculated based on the hydrodynamic radii calculations of Armstrong et al.[29] and the Stokes−Einstein equation (eq 2). Swelling-based estimates of solute diffusivities and diffusivity-based estimates of mesh radii were calculated using a modified multiscale diffusion model (eq 3).[14,15] The R scripts used to calculate structural values and diffusion coefficients are available in the Supporting Information.

$$D_0 = \frac{k_b T}{6\pi\eta r_s} \quad (2)$$

In eq 2, D_0 is the diffusivity of the solute in solution, k_b is the Boltzmann constant (1.38 × 10^{-23} J/K), T is the temperature (298 K), η is the solution's viscosity (0.00089 Pa s), and r_s is the hydrodynamic radius of the solute.

https://doi.org/10.1021/acs.macromol.1c01752
Macromolecules 2021, 54, 10477−10486

$$\frac{D}{D_0} = \mathrm{erf}\left(\frac{r_{FVW}}{r_s}\right)\exp\left[-1 \times \left(\frac{r_s}{r_{FVW}}\right)^3\left(\frac{\varphi_s}{1-\varphi_s}\right)\right] + \mathrm{erfc}\left(\frac{r_{FVW}}{r_s}\right)\exp\left[\frac{-\pi}{4} \times \left(\frac{r_s + r_f}{r_{mesh}}\right)^2\right] \quad (3)$$

In eq 3, D is the diffusivity of the solute in the hydrogel, r_{FVW} is the radius of free volume voids in water (0.269 nm), and r_f is the fiber radius of the polymer in water (for PVA, 0.55 nm).

Statistics and Data Availability. Swelling experiments were performed in triplicate with two batches per formulation (n = 6). FRAP experiments on solutes in solution were performed in triplicate (n = 3). FRAP experiments in hydrogel were performed with three samples from each of two batches and three scans at different positions in the hydrogel (n = 18). All values are represented as mean ± standard deviation. Paired t tests were performed using GraphPad Prism 9 software (GraphPad Software, San Diego, CA). Statistical significance was evaluated at $P < 0.05$. Full quantitative data are available in the Supporting Information.

RESULTS

To evaluate the effects of hydrogel design on solute transport, we prepared 18 formulations of PVA hydrogels and then incubated each formulation in solutions of fluorescein, three sizes of FITC-dextran, or three sizes of FITC-PEG. Solute diffusion was analyzed via FRAP experiments, and diffusion coefficients for each solute formulation pairing were first calculated via the FRAP analysis program developed by Jönsson et al.[27] and then recalculated with a novel, high-throughput modification of their program. Mesh transport theory was used to interpret the relationships between diffusion coefficients and the properties of each solute-hydrogel pairing.

Samples of eighteen PVA hydrogel formulations were synthesized with three different initial polymer volume fractions (φ_0) and six different degrees of polymerization between junctions (N_j), each in two batches to mitigate batch-dependent effects. Swelling profiles of each formulation were characterized as previously described.[28] For this study, hydrogel formulations were characterized by their mesh radii,[15] which were calculated from synthesis-based structural parameters and the swollen polymer volume fraction of each hydrogel formulation (eq 1 and Table S1).

The diffusion coefficient of each solute in aqueous solution (10 μM in PBS) was measured using the Jönsson program[27] (Figure 1). Literature-based diffusion coefficients for each solute were calculated from their hydrodynamic radii using the Stokes–Einstein equation as described in the Methods section (eq 2 and Table S2). In free solution, both the FRAP-measured and Stokes–Einstein-estimated diffusion coefficients decreased with an increasing hydrodynamic radius for both FITC-dextrans and FITC-PEGs. The large difference between modeled and measured values for fluorescein may be a result of fluorescein's tendency to form dimers in aqueous solution.[30] Overall, these results confirm that FRAP experiments analyzed with the Jönsson program reliably measure solute diffusion coefficients in solution, justifying further application of FRAP analysis to solute diffusion in hydrogels.

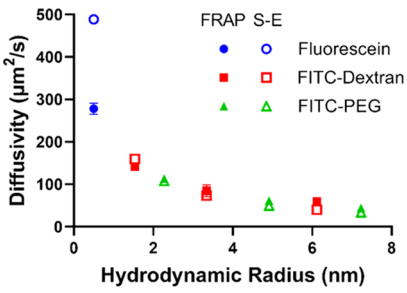

Figure 1. Diffusivity of fluorescent solutes in solution. Fluorescent recovery after photobleaching (FRAP) measurements of the diffusivity of fluorescein, three sizes of FITC-dextran, and three sizes of FITC-PEGs in aqueous solution were compared to diffusion coefficients predicted from the Stokes–Einstein (S–E) equation (eq 2). Error bars represent standard deviations (n = 3).

Automation of the FRAP Analysis Program. The FRAP analysis MATLAB program developed by Jönsson et al.[27] guides the user through one of the most computationally robust methods for analyzing FRAP data[21] based on a Hankel transform of spatial intensity data. The program is well suited for analyzing FRAP experiments on a single solute in a hydrogel and includes capabilities for measuring immobile solute fractions as well as tracking the bleach spot movement due to convection, which was necessary for analyzing diffusion coefficients in solution. However, the program is designed to analyze a single FRAP experiment at a time. Multiple interactive steps are required for each FRAP experiment, and analytical results are presented but not saved for later interpretation. For our goals of characterizing over 2000 FRAP experiments, experiment-by-experiment analysis quickly became laborious. More than 150 h were spent analyzing the current dataset with the program despite the standardized parameters for all FRAP experiments in hydrogels.

Our appreciation for the precision of the spatial Hankel analysis method and frustration with the Jönsson program's user interface motivated us to create a streamlined version of the program for high-throughput analysis of solute diffusion in hydrogels. The modified program automatically analyzes a folder of standardized FRAP experiments, saves all results to a spreadsheet, and exports the data-fit graphs to a folder for review (MATLAB program available in the Supporting Information). Using the modified program, all the FRAP experiments in hydrogels were reanalyzed in less than 3 h with only brief (~2 min) user involvement to initiate the analysis. Conversion from the manual analysis method to an automated method resulted in at least a 50-fold reduction in total analysis time and over a 500-fold reduction in person hours of analytical work.

Comparison of diffusion coefficients measured via the manual and automated programs show a strong 1:1 correlation across all solute formulation pairings (Figure 2A), with the greatest percent difference of 4.9% in the most transport-restrictive hydrogel (φ_0 = 0.100, N_j = 20) with a 4 kDa FITC-dextran solute (Figure 2B). A paired t test of the automated and manual data showed a nonsignificant difference (p = 0.89). With such minimal changes to the measured diffusion coefficient values and a 50-fold reduction in batch analysis time and effort, we anticipate that the modified high-throughput program will be a valuable tool for improving understanding of solute transport in hydrogels via FRAP experiments.

Immobilization of Solutes within the Hydrogels. Unlike solute-hydrogel systems where the solutes are introduced before hydrogel formation and therefore possibly partially entrapped by the network formation reaction, all solutes in these studies entered the preformed hydrogels via

https://doi.org/10.1021/acs.macromol.1c01752
Macromolecules 2021, 54, 10477–10486

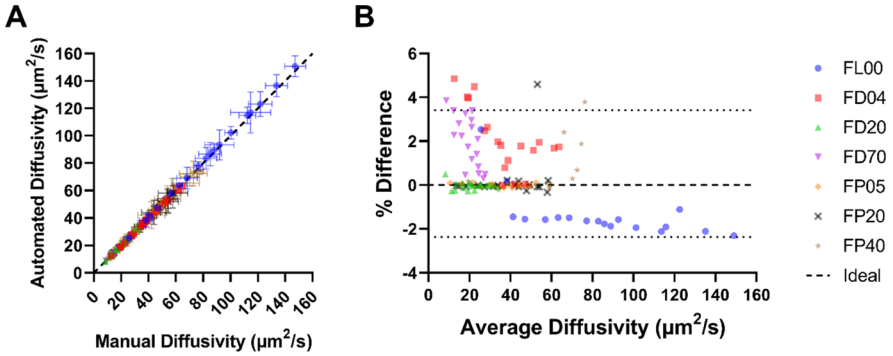

Figure 2. Comparison of manual and automated diffusivity analysis methods. (A) Direct comparison of manual and automated results. Error bars represent standard deviations (n = 18). (B) Bland–Altman graph clarifies the percent differences between manual and automated results. Positive percent differences represent higher manual values than automated values. Dotted lines represent 95% limits of agreement. FL00, fluorescein; FD04, 4 kDa FITC-dextran; FD20, 20 kDa FITC-dextran; FD70, 70 kDa FITC-dextran; FP05, 5 kDa FITC-PEG; FP20, 20 kDa FITC-PEG; FP40, 40 kDa FITC-PEG.

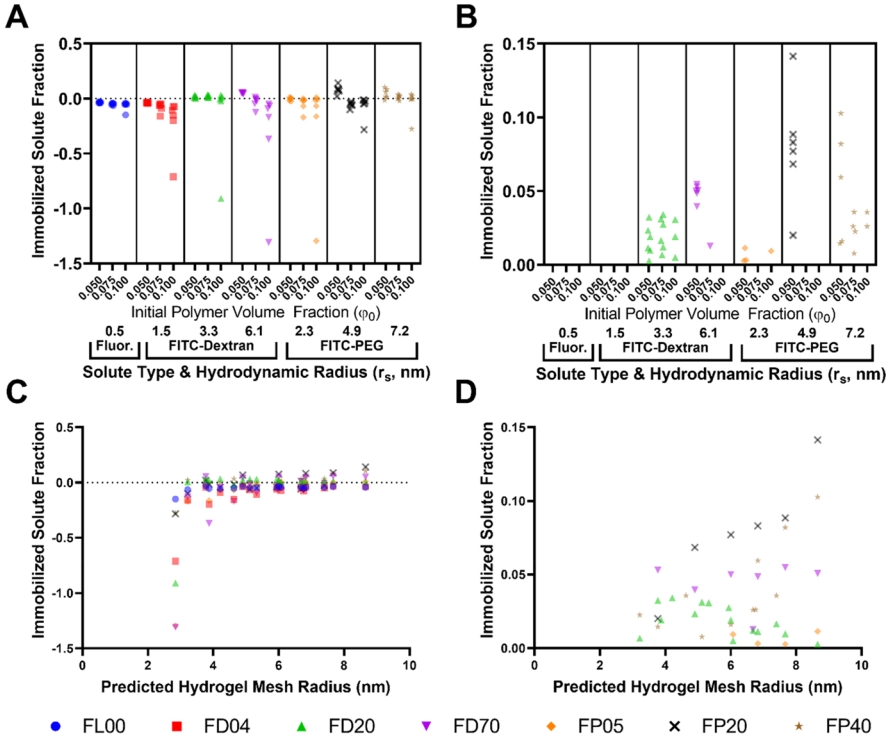

Figure 3. Measured immobilized solute fraction dependence on solute characteristics and hydrogel mesh radii. Immobilized solute fractions calculated using Fit 2 analysis of FRAP experiments grouped by solute characteristics and initial polymer volume fraction (A, B) or hydrogel mesh radius (C, D) with subset graphs to show only positive immobilized solute fractions (B, D). Error bars were omitted for visual clarity, and points were shown at 50% transparency to help visualize repeated values. FL00, fluorescein; FD04, 4 kDa FITC-dextran; FD20, 20 kDa FITC-dextran; FD70, 70 kDa FITC-dextran; FP05, 5 kDa FITC-PEG; FP20, 20 kDa FITC-PEG; FP40, 40 kDa FITC-PEG.

diffusion from a bulk solution. Because the solutes were introduced via diffusion, we hypothesized that negligible solute immobilization, or physical entrapment, would occur within the hydrogel regardless of solute and hydrogel characteristics. We tested our hypothesis by using a two-parameter fit of the FRAP experiment data that identifies the immobile fraction of solute in each hydrogel formulation. Whereas the standard Fit 1 considered only a single diffusion coefficient parameter, Fit 2 incorporated a second parameter, the immobilized solute fraction. Fit 2 calculated the immobilized solute fraction based on any persistent reduction in fluorescence within the bleached spot after the system returns to diffusive equilibrium.

Immobilized solute fractions calculated via Fit 2 were compared based on solute size and type (Figure 3A,B) and hydrogel mesh radius (Figure 3C,D). At least one unrealistic negative immobilized solute fraction was calculated for each solute (Figure 3A) and each hydrogel formulation (Figure 3C), and all negative values were interpreted as diffusion without immobilization. Notably, all fluorescein and 4 kDa FITC-dextrans had negative immobilized solute fractions, suggesting that these solutes were consistently too small (and effectively spherical) to be immobilized. The largest negative immobilized solute fractions correspond to the most restrictive hydrogel (φ_0 = 0.100, N_j = 20), which could be an analytical artifact caused by the need for longer recovery

https://doi.org/10.1021/acs.macromol.1c01752
Macromolecules 2021, 54, 10477−10486

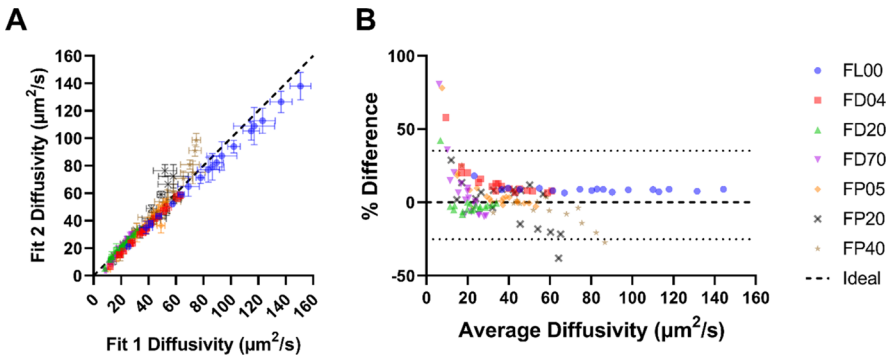

Figure 4. Comparison of diffusion coefficients from analysis models neglecting (Fit 1) or including (Fit 2) the possibility of solute immobilization. (A) Direct comparison of Fit 1 and Fit 2 diffusion coefficients. Error bars represent standard deviations (n = 18). (B) Bland–Altman graph clarifies the percent differences between Fit 1 and Fit 2 diffusion coefficients. Positive percent differences represent higher Fit 1 values than Fit 2 values. Dotted lines represent 95% limits of agreement. FL00, fluorescein; FD04, 4 kDa FITC-dextran; FD20, 20 kDa FITC-dextran; FD70, 70 kDa FITC-dextran; FP05, 5 kDa FITC-PEG; FP20, 20 kDa FITC-PEG; FP40, 40 kDa FITC-PEG.

periods to reach diffusive equilibrium (Figure S1). Regarding how solute properties affect immobilized solute fractions, FITC-dextran shows an apparent trend of increasing immobilized fraction with increasing size, but the FITC-PEGs do not match the trend, with the largest immobilized solute fraction observed in the 20 kDa FITC-PEG (Figure 3B).

The dependence of the positive immobilized solute fractions on mesh radius does not show consistent trends across all solutes (Figure 3D). However, further analysis of the underlying data revealed that six of the seven 70 kDa FITC-dextran solute-formulation parings with positive immobilized solute fractions were in low initial polymer volume fraction hydrogels (φ_0 = 0.050). Similarly, all six of the hydrogel formulations with positive immobilization of 20 kDa FITC-PEG were made using the low initial polymer volume fraction. These results suggest that the initial polymer volume fraction somehow has a greater impact on immobilized solute fraction than the mesh radius, with mesh radius possibly having a secondary effect as suggested by the positive trend observed for 20 kDa FITC-PEG but not for 70 kDa FITC-dextran.

The lack of positive immobilized solute fractions in the most restrictive hydrogel and the dependence on initial polymer volume fraction suggests that relatively open, spacious networks and possibly a wide distribution of effective mesh radii are needed to immobilize solutes that are introduced by diffusion. Immobilization of solutes that were introduced via diffusion may indicate that the solutes penetrated until they were entrapped, possibly by an unusually small local mesh radius and/or unsuccessful reptation of the solute's polymeric segments through the network. From these results, we conclude that the design of hydrogels for the control of solute diffusion must also address how structural parameters affect solute immobilization.

Secondarily, diffusion coefficients calculated using Fit 1 and Fit 2 were compared to understand if adding solute immobilization to the analytical model had any effect on the measured diffusivity (Figure 4). A paired t test of the entire dataset found the difference between fits to be marginally nonsignificant (P = 0.0518), but there were clear solute-specific deviations for 20 and 40 kDa FITC-PEGs favoring higher diffusion coefficients with Fit 2 (Figure 4A). These deviations correspond to the solute-formulation pairings with the greatest immobilized fractions. At the lowest diffusivities associated with the most restrictive hydrogel formulation (φ_0 = 0.100, N_j = 20), the percent differences between calculated diffusivities were exceptionally high, with the 70 kDa FITC-dextran at an 80% difference (Figure 4B). The large percent differences at low diffusivities correspond to FRAP experiments that were conducted with insufficient time for the system to reach diffusive equilibrium (Figure S1), rendering estimates of the immobilized solute fractions for those experiments nonsensical. Overall, these results suggest that the comparison of Fit 1 and Fit 2 solute diffusion coefficients in hydrogels yields negligible global differences. While Fit 2 more accurately addresses situations where there is a significant immobile fraction, the additional requirement for the system to reach diffusive equilibrium means that the less-demanding Fit 1 is a more robust tool for characterizing diffusion coefficients from FRAP experiments in hydrogels.

Comparison of FRAP Diffusivity Data with Mesh Transport Model Predictions. Based on the fundamental assumptions included in mesh transport theory, solute diffusivity in hydrogels is expected to (i) decrease with solute size, (ii) never exceed the diffusivity observed in free solution, and (iii) predict a consistent mesh radius for each hydrogel formulation regardless of solute size and type. We experimentally evaluated these three expectations in hydrogels with varying structural parameters and mesh radii. To summarize measurements and modeled predictions of diffusivity, normalized diffusivity, and mesh radius for 7 solutes in 18 hydrogel formulations, we compared the most permissive hydrogel formulation (φ_0 = 0.050, N_j = 70), the median hydrogel formulation (φ_0 = 0.075, N_j = 50), and the second-most restrictive hydrogel formulation (φ_0 = 0.100, N_j = 30) to describe a wide range of hydrogel formulation-dependent diffusivity profiles (Figure 5).

From the comparisons of solute diffusivities and solute hydrodynamic radii in all three hydrogel formulations (Figure 5A–C), we conclude that the model overestimated the diffusivity of smaller molecules (below 4 nm). The ratio of modeled to measured diffusivity grew larger as measured diffusivities greatly decreased in the more restrictive hydrogel formulations. The fluorescein and FITC-dextran measurements appeared to match the modeled decrease in diffusivity with solute size, but the FITC-PEGs broke the trend by increasing in measured diffusivity with increasing solute sizes. When diffusivity was normalized by the free solution diffusivity of each solute, the normalized diffusivities of small molecules were overestimated again by the model (Figure 5D–F). For both the FITC-dextran and FITC-PEG solute groups,

https://doi.org/10.1021/acs.macromol.1c01752
Macromolecules 2021, 54, 10477–10486

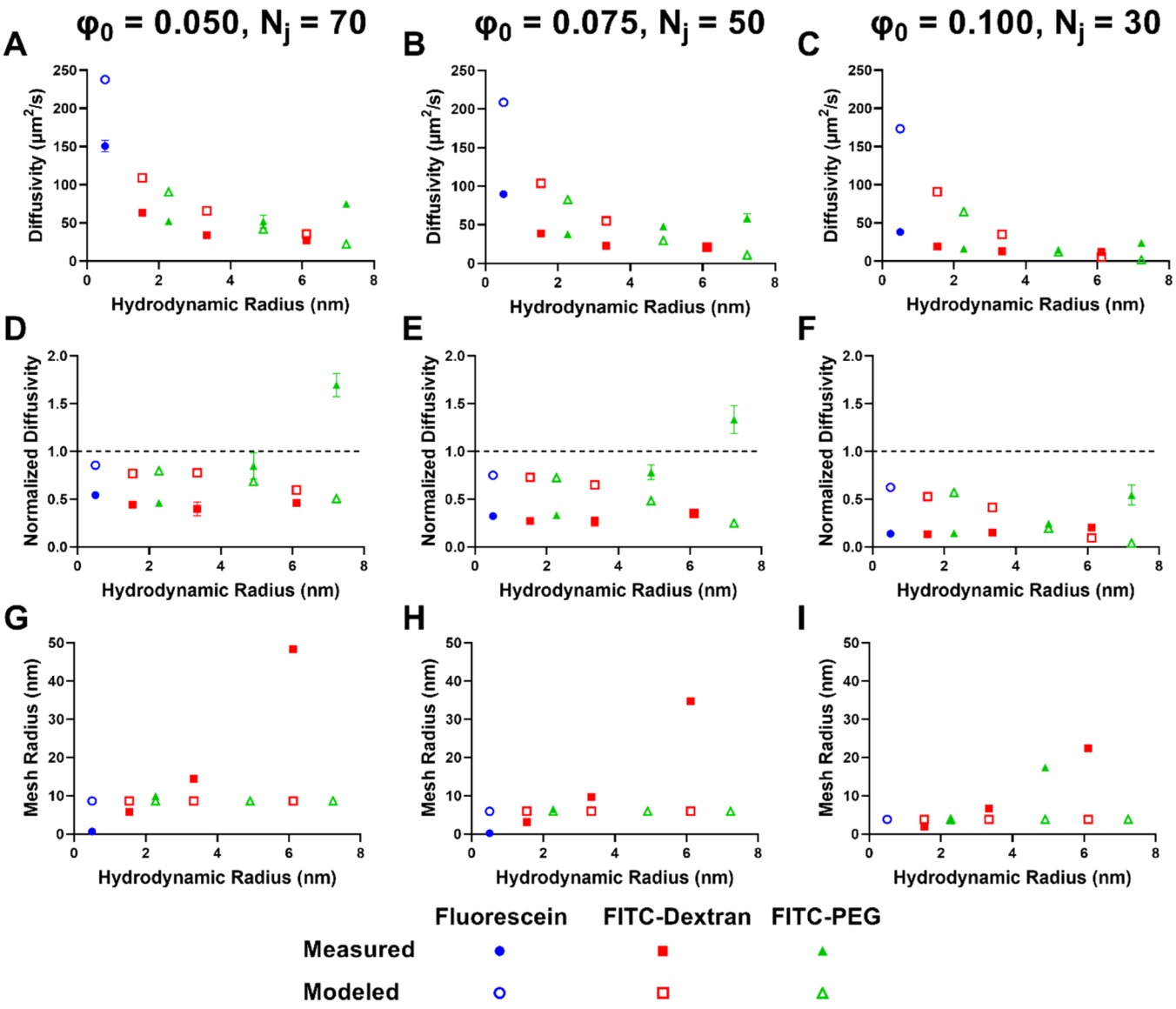

Figure 5. Calculation of normalized diffusivities and mesh radii from solute diffusivities in permissive, moderate, and restrictive hydrogel formulations. For selected permissive (φ_0 = 0.050, N_j = 70), moderate (φ_0 = 0.075, N_j = 50), and restrictive (φ_0 = 0.100, N_j = 30) hydrogel formulations, diffusivities were measured from FRAP analysis and modeled by the modified multiscale diffusion model (A−C), normalized diffusivities were calculated based on free diffusivities in solution (D−F), and mesh radii were calculated by inverting the modified multiscale diffusion model (G−I). Diffusivity error bars represent standard deviation (n = 18), and normalized diffusivity error bars were calculated via propagation of error from diffusivity standard deviations and free solute standard deviations (n_{free} = 3).

normalized diffusivities increased with hydrodynamic radius, unlike the model-predicted reduction in solute diffusivity with increasing size. Surprisingly, in the permissive (Figure 5D) and moderate (Figure 5E) hydrogel formulations, the normalized diffusivity of the 40 kDa FITC-PEG was greater than one, suggesting that the diffusion of the 40 kDa FITC-PEG in a PVA hydrogel is faster than in an aqueous solution.

The trends in diffusivity and normalized diffusivity highlight the inadequacy of the model to describe solute transport in hydrogels. Specifically, the exceptional normalized diffusivity coefficients of the 40 kDa FITC-PEG in hydrogels require a robust reconsideration of the relevant phenomena. Immediate points of consideration include the solute concentration within the hydrogel, the distribution of solute sizes within the hydrogel, and the shape of the solute. A separate, supplementary partition coefficient experiment (Figure S4) showed below-unity partition coefficients for larger solutes (FP20, FP40, and FD70) in all formulations, suggesting that there may be a screening effect based on solute size. However, the different hydrogel formulations had marginal effects on the partition coefficients, and the partition coefficients were higher for FP40 than they were for FD70, so lower concentrations and size-based screening alone cannot fully account for the unique behavior of the 40 kDa FITC-PEG. These results suggest that the shape difference between FITC-PEG and FITC-dextran played a significant role. Specifically, since FITC-PEG is linear and FITC-dextran is globular, a large FITC-PEG molecule is most likely to diffuse in a hydrogel via reptation.[31,32] In effect, it is likely that a combination of lower concentrations, downshifted solute sizes, and linear PEG reptation within the hydrogels create the unexpected experimental results shown in Figure 6A−F.

The estimation of mesh radius from solute diffusion coefficients in each hydrogel formulation disrupts the third

https://doi.org/10.1021/acs.macromol.1c01752
Macromolecules 2021, 54, 10477−10486

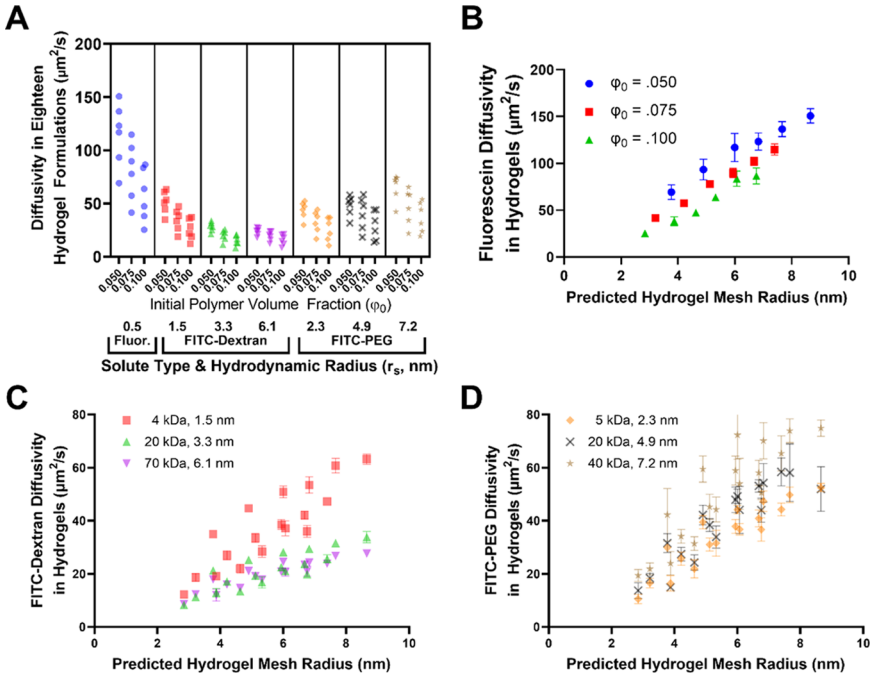

Figure 6. Solute diffusivity in hydrogels varies with solute size and type as well as hydrogel mesh radius. Solute diffusivities in hydrogels were grouped by solute size and type (A) to visualize their solute-dependent values and distributions. Error bars excluded for visual clarity. Solute diffusivities were then organized in response to hydrogel mesh radii, with fluorescein diffusivities further separated by initial polymer volume fractions to highlight the associated trends (B). FITC-dextran diffusivities (C) and FITC-PEG diffusivities (D) were graphed separately for clarity. Error bars represent standard deviations (n = 18).

assumption that mesh radius is consistent within a hydrogel formulation (Figure 5G−I). Measured mesh radii, which were calculated from normalized diffusion coefficients and an inverted form of the modified multiscale diffusion model (eq 3), consistently increased with solute radii across all formulations. One interpretation of this result is that the PVA hydrogels have a distribution of mesh radii, and all the solutes have a size-dependent lower limit for the mesh radius they can interact with, such as in size exclusion chromatography. Alternatively, the model may be poorly equipped or not optimized for evaluating the relationship between solute size and mesh radius, especially since it has not been previously tested with simultaneous variations in hydrogel formulation, solute size, and solute type.[14] Notably, low values of the fluorescein normalized diffusivity yielded nonreal mesh radii values (Figure 5I), and measured mesh radii for the 40 kDa FITC-PEGs were either exceptionally high (22,600 nm for φ_0 = 0.050, N_j = 20) or negative if the normalized diffusion coefficient was greater than one. These cases demonstrate the practical limitations of the modified multiscale diffusion model in evaluating unexpected solute behavior within hydrogels. Taken together, these experimental results and modeling comparisons provide evidence that solute transport in hydrogels is not simply influenced by solute sizes and hydrogel mesh radii, and future diffusion modeling efforts must address additional possible interactions between solutes and the hydrogel, such as shape-dependent reptation.

Control of Solute Transport in Hydrogels. Overarching control of solute diffusivities is one of the primary goals of hydrogel structural design and swollen polymer network modeling.[15,20,28] To summarize the practical utility of this study, we considered the range of diffusivities for each solute in the tested hydrogel formulations (Figure 6A) as well as how mesh radii affected solute diffusivities (Figure 6B−D). Fluorescein and FITC-dextrans shared a trend of decreasing range and decreasing diffusivities with increasing solute size, but the FITC-PEGs showed negligible changes in the ranges or values of diffusivities and a slight increase in overall diffusivities with increasing solute size (Figure 6A). Despite these inconsistencies across solute groups, all solutes showed a general trend of increasing diffusivity with increasing hydrogel mesh radius (Figure 6B−D). However, the stratification of the fluorescein trends by initial polymer volume fraction (Figure 6B) show that mesh radius is not a universal predictor of whether a solute will have a higher diffusivity in one hydrogel formulation over another. In Figure 6C, a similar stratification can be observed for 4 kDa FITC-dextrans, and the difference between the 20 and 70 kDa FITC-dextrans is negligible. The FITC-PEGs (Figure 6D) have a stronger overall response to the hydrogel mesh radius than the FITC-dextrans that are not weakened at higher solute sizes. These results suggest a need for more consideration of the solute type and more precise parameterization relating hydrogel structural properties to solute transport.

■ DISCUSSION

With this work, we aimed to use multivariate, high-throughput experimentation and analysis of solute diffusivity in hydrogels to challenge model-encoded assumptions about solute and hydrogel properties. The automated analysis software for standardized FRAP experiments created for this project will continue to accelerate FRAP experimental analysis in our research and as a widely accessible, modifiable MATLAB program available online (see Supporting Information). The modified program is optimized for solute diffusion in hydrogels, as demonstrated by its inability to analyze the diffusion coefficients of solutes in free solution, where bulk

https://doi.org/10.1021/acs.macromol.1c01752
Macromolecules 2021, 54, 10477−10486

convection moved the bleached spot away from the center of the images (Figure S3). However, the 50-fold reduction in analysis time will compound the efficiency of future experiments, and results can be corroborated by the slower Jönsson FRAP analysis program and other established methods for evaluating diffusion coefficients from FRAP data.

The different trends relating solute size to diffusivity in hydrogels for FITC-dextrans and FITC-PEGs undermine the modeling assumption that diffusing solutes can be treated as noninteracting hard spheres defined by their hydrodynamic radius. The differences observed in hydrogels are enhanced by comparisons with diffusion in free solution, where both FITC-dextrans and FITC-PEGs closely matched Stokes−Einstein-based predictions. The hydrogel-dependent differences therefore suggest that either chemistry-dependent solute−network interactions, such as hydrogen bonding,[33,34] or solute structure-dependent interactions, such as movement via reptation,[35] contribute significantly to effective diffusivities of FITC-dextrans, FITC-PEGs, or both in hydrogels. Comparable partition coefficients between FITC-dextrans and FITC-PEGs (Figure S4), both less than 1, suggest that differences in chemical interactions are also negligible. Instead, solute-structure-dependent interactions, also unaddressed by the current mesh transport models, may cause the observed differences between FITC-dextrans and FITC-PEGs. PEGs are linear molecules with an ellipsoid aspect ratio of 2.13,[36] whereas dextrans have a more globular random coil shape,[37] suggesting that FITC-PEGs may exhibit polymeric reptation and enhanced anisotropic diffusion along their major axis within a restrictive hydrogel environment. Regardless of the specific mechanism behind the differences, the comparison between FITC-dextrans and FITC-PEGs as well as the multiscale diffusion model calculating negative values for FITC-PEGs and nonreal numbers for fluorescein indicate that current models for solute diffusivity in hydrogels overemphasize and incorrectly generalize the effects of solute size. Solute shape anisotropy and movement via reptation must be addressed in the next generation of mesh transport models.

Variations in hydrogel formulation based on the initial polymer volume fraction and the degree of polymerization between junctions affected both the diffusion coefficients of solutes and the (physically) immobilized solute fractions of large solutes. Figure 6B shows that mesh radius can be used to describe general trends in solute diffusivities, but the underlying control variables of initial polymer volume fraction and degree of polymerization further influence solute diffusivities, creating distinct subtrends in the relationship between mesh radii and solute diffusivities. These results broadly suggest that simple models correlating solute diffusivity to mesh sizes, such as the molecular size exclusion method,[9,10,13] are likely overfitted and therefore misattribute other hydrogel structural changes to changes in mesh sizes.

Four of the solutes studied here have hydrodynamic radii within the ranges of hydrogel mesh radii (3−9 nm), yet no clear interactions or changes in trends were observed at the solute−mesh crossover points, further suggesting that mesh radius is an abstraction rather than a direct influence on solute diffusion in hydrogels. It may prove more effective and generally applicable to focus on the relationships between solute diffusivities and specific, synthesis-controlled hydrogel properties such as the initial polymer volume fraction and degree of polymerization between junctions. However, even these parameters may overgeneralize important structural properties, such as the distribution of degrees of polymerization between junctions in a hydrogel. A large, standardized dataset of solute diffusivities in many hydrogel formulations, facilitated by the high-throughput FRAP analysis method, will help to identify which hydrogel structural parameters have the greatest effects on solute diffusivities.

Limitations of the current study include the rate and period of FRAP video capture per experiment, the choice of hydrogel formulations and solutes studied, and the narrow modeling approach used. As described in the comparison of Fit 1 and Fit 2 analysis methods, the pairings of large solutes and highly restrictive hydrogels led to slow diffusion that did not reach equilibrium within the standard FRAP experimental period. For this study, general conclusions were drawn regarding solute diffusion in hydrogels based on glutaraldehyde-cross-linked PVA hydrogels with variations in two structural parameters, possibly leading to conclusions that do not apply in other hydrogel systems. Finally, the modeling approach did not consider alternatives to the swollen polymer network model and the multiscale diffusion model, even though many competing models exist to describe solute diffusion in hydrogels.[38] We provided premodeling data as well as commented code for the modeling calculations through the Supporting Information to facilitate reanalysis of the experimental dataset using new or alternative modeling methods in the future.

The high-throughput analysis method for solute diffusivities in hydrogels described here creates a platform for investigating solute and hydrogel properties not studied here. In addition to the initial polymer volume fractions and degrees of polymerization between junctions controlled here, we have recently discussed how changing a hydrogel's junction functionality and frequency of chain-end defects might affect solute diffusivity.[15] In particular, the distinction between mesh size and mesh radius is trivial without manipulating junction functionalities. As discussed above, explicit studies of solute shape on diffusivity in hydrogels may lead to more generalizable models, potentially through the use of gold spherical nanoparticles and nanorods.[39,40]

FRAP experiments do not address solute partitioning between bulk aqueous solution and a hydrogel or gradient-driven diffusion, which are both critical topics for drug delivery applications. Partitioning and hydrogel interfacial studies will prove instructive to FRAP experiments by revealing how and why solutes are excluded from a hydrogel,[6,24] and detailed partitioning studies will reveal whether the solute size distributions within a hydrogel are representative of the size distributions found in bulk solution. Furthermore, the diffusion coefficients calculated from release studies represent gradient-driven diffusion,[7,16] and it remains unclear whether the local diffusion coefficients measured by FRAP experiments in hydrogels consistently correlate to release rates. Future work that coordinates partition, release, and FRAP experiments will improve our understanding of solute diffusion in and from hydrogels.

CONCLUSIONS

Fluorescence recovery after photobleaching experiments are a powerful tool for analyzing solute diffusivity within hydrogels. This article presents a high-throughput method for FRAP analysis that is used to evaluate structure-diffusivity relationships in 126 pairings of solutes and hydrogel formulations. Size-dependent trends were not conserved across solute types.

https://doi.org/10.1021/acs.macromol.1c01752
Macromolecules 2021, 54, 10477−10486

FITC-dextrans generally reduced in diffusivity with solute size, but larger FITC-PEGs diffused in hydrogels at greater speeds than smaller FITC-PEGs, possibly due to increasing shape anisotropy and movement via reptation. Similarly, the effects of varying hydrogel formulations on solute diffusivities could not be reduced to simple size-based effects. Simultaneous variation of the initial polymer volume fraction and the degree of polymerization between junctions had distinct effects on solute diffusivities that could not be generalized based on mesh radii. We anticipate that these results and an improved method for high-throughput analysis of FRAP experiments on solutes diffusing in hydrogels will motivate further studies on solute and hydrogel properties, ultimately improving hydrogel design for biomedical applications.

■ ASSOCIATED CONTENT

Supporting Information

The Supporting Information is available free of charge at https://pubs.acs.org/doi/10.1021/acs.macromol.1c01752.

DOI links to code, protocols, and raw data for this project as well as tables of hydrogel and solute properties; (Figures S1−S3) more context on FRAP analysis methods (PDF)

■ AUTHOR INFORMATION

Corresponding Author

Nicholas A. Peppas − *Department of Biomedical Engineering and Departments of Surgery and Pediatrics, Dell Medical School, University of Texas, Austin, Texas 78712, United States; McKetta Department of Chemical Engineering and Division of Molecular Therapeutics and Drug Delivery, College of Pharmacy, University of Texas, Austin, Texas 78712, United States;* orcid.org/0000-0003-0894-5626; Email: peppas@che.utexas.edu

Author

Nathan R. Richbourg − *Department of Biomedical Engineering, University of Texas, Austin, Texas 78712, United States;* orcid.org/0000-0002-5091-3321

Complete contact information is available at: https://pubs.acs.org/10.1021/acs.macromol.1c01752

Notes

The authors declare no competing financial interest.

■ ACKNOWLEDGMENTS

The authors would like to acknowledge Mauricio Gonzalez and Akhila Ravikumar for assistance with the manual analysis of FRAP data in hydrogels, Anna Webb for training on the Zeiss LSM 710 Confocal Microscope at the UT Center for Biomedical Research Support, and ChE and BME Ph.D. students Andrew Murphy and Dana Jenkins for providing feedback on the manuscript. Support for this work was provided by the National Science Foundation under award number DGE-1610403 (N.R.R.) and the National Institute of Biomedical Imaging and Bioengineering of the National Institutes of Health under grant R01 EB022025 (N.A.P.). The content is solely the responsibility of the authors and does not necessarily represent the official views of the NIH or the NSF.

■ REFERENCES

(1) Bernhard, S.; Tibbitt, M. W. Supramolecular engineering of hydrogels for drug delivery. *Adv. Drug Delivery Rev.* **2021**, *171*, 240−256.

(2) Mandal, A.; Clegg, J. R.; Anselmo, A. C.; Mitragotri, S. Hydrogels in the clinic. *Bioeng. Transl. Med.* **2020**, *5*, No. e10158.

(3) Thakor, J.; Ahadian, S.; Niakan, A.; Banton, E.; Nasrollahi, F.; Hasani-Sadrabadi, M. M.; Khademhosseini, A. Engineered hydrogels for brain tumor culture and therapy. *Bio-Des. Manuf.* **2020**, *3*, 203−226.

(4) Wechsler, M. E.; Stephenson, R. E.; Murphy, A. C.; Oldenkamp, H. F.; Singh, A.; Peppas, N. A. Engineered microscale hydrogels for drug delivery, cell therapy, and sequencing. *Biomed. Microdevices* **2019**, *21*, 31.

(5) Hagman, J.; Lorén, N.; Hermansson, A.-M. Probe diffusion in κ-carrageenan gels determined by fluorescence recovery after photobleaching. *Food Hydrocolloids* **2012**, *29*, 106−115.

(6) Kotsmar, C.; Sells, T.; Taylor, N.; Liu, D. E.; Prausnitz, J. M.; Radke, C. J. Aqueous Solute Partitioning and Mesh Size in HEMA/MAA Hydrogels. *Macromolecules* **2012**, *45*, 9177−9187.

(7) Liu, D. E.; Kotsmar, C.; Nguyen, F.; Sells, T.; Taylor, N. O.; Prausnitz, J. M.; Radke, C. J. Macromolecule Sorption and Diffusion in HEMA/MAA Hydrogels. *Ind. Eng. Chem. Res.* **2013**, *52*, 18109−18120.

(8) Hadjiev, N. A.; Amsden, B. G. An assessment of the ability of the obstruction-scaling model to estimate solute diffusion coefficients in hydrogels. *J. Controlled Release* **2015**, *199*, 10−16.

(9) Jimenez-Vergara, A. C.; Lewis, J.; Hahn, M. S.; Munoz-Pinto, D. J. An improved correlation to predict molecular weight between crosslinks based on equilibrium degree of swelling of hydrogel networks. *J. Biomed. Mater. Res., Part B* **2018**, *106*, 1339−1348.

(10) Munoz-Pinto, D. J.; Samavedi, S.; Grigoryan, B.; Hahn, M. S. Impact of secondary reactive species on the apparent decoupling of poly(ethylene glycol) diacrylate hydrogel average mesh size and modulus. *Polymer* **2015**, *77*, 227−238.

(11) Offeddu, G. S.; Axpe, E.; Harley, B. A. C.; Oyen, M. L. Relationship between permeability and diffusivity in polyethylene glycol hydrogels. *AIP Adv.* **2018**, *8*, 105006.

(12) Barnhouse, V.; Petrikas, N.; Crosby, C.; Zoldan, J.; Harley, B. Perivascular Secretome Influences Hematopoietic Stem Cell Maintenance in a Gelatin Hydrogel. *Ann. Biomed. Eng.* **2021**, *49*, 780−792.

(13) Browning, M. B.; Wilems, T.; Hahn, M.; Cosgriff-Hernandez, E. Compositional control of poly(ethylene glycol) hydrogel modulus independent of mesh size. *J. Biomed. Mater. Res., Part A* **2011**, *98A*, 268−273.

(14) Axpe, E.; Chan, D.; Offeddu, G. S.; Chang, Y.; Merida, D.; Hernandez, H. L.; Appel, E. A. A Multiscale Model for Solute Diffusion in Hydrogels. *Macromolecules* **2019**, *52*, 6889−6897.

(15) Richbourg, N. R.; Ravikumar, A.; Peppas, N. A. Solute Transport Dependence on 3D Geometry of Hydrogel Networks. *Macromol. Chem. Phys.* **2021**, *222*, 2100138.

(16) Rehmann, M. S.; Skeens, K. M.; Kharkar, P. M.; Ford, E. M.; Maverakis, E.; Lee, K. H.; Kloxin, A. M. Tuning and Predicting Mesh Size and Protein Release from Step Growth Hydrogels. *Biomacromolecules* **2017**, *18*, 3131−3142.

(17) Zustiak, S. P.; Boukari, H.; Leach, J. B. Solute diffusion and interactions in cross-linked poly(ethylene glycol) hydrogels studied by Fluorescence Correlation Spectroscopy. *Soft Matter* **2010**, *6*, 3609−3618.

(18) Hegab, R. A.; Pardue, S.; Shen, X.; Kevil, C.; Peppas, N. A.; Caldorera-Moore, M. E. Effect of network mesh size and swelling to the drug delivery from pH responsive hydrogels. *J. Appl. Polym. Sci.* **2020**, *137*, 48767.

(19) Canal, T.; Peppas, N. A. Correlation between mesh size and equilibrium degree of swelling of polymeric networks. *J. Biomed. Mater. Res.* **1989**, *23*, 1183−1193.

(20) Richbourg, N. R.; Peppas, N. A. The swollen polymer network hypothesis: Quantitative models of hydrogel swelling, stiffness, and solute transport. *Prog. Polym. Sci.* **2020**, *105*, 101243.

(21) Lorén, N.; Hagman, J.; Jonasson, J. K.; Deschout, H.; Bernin, D.; Cella-Zanacchi, F.; Diaspro, A.; McNally, J. G.; Ameloot, M.; Smisdom, N.; Nydén, M.; Hermansson, A.-M.; Rudemo, M.; Braeckmans, K. Fluorescence recovery after photobleaching in material and life sciences: putting theory into practice. *Q. Rev. Biophys.* **2015**, *48*, 323−387.
(22) Deschout, H.; Raemdonck, K.; Demeester, J.; De Smedt, S. C.; Braeckmans, K. FRAP in Pharmaceutical Research: Practical Guidelines and Applications in Drug Delivery. *Pharm. Res.* **2014**, *31*, 255−270.
(23) Kosto, K. B.; Deen, W. M. Diffusivities of macromolecules in composite hydrogels. *AIChE J.* **2004**, *50*, 2648−2658.
(24) Dursch, T. J.; Taylor, N. O.; Liu, D. E.; Wu, R. Y.; Prausnitz, J. M.; Radke, C. J. Water-soluble drug partitioning and adsorption in HEMA/MAA hydrogels. *Biomaterials* **2014**, *35*, 620−629.
(25) Berk, D. A.; Yuan, F.; Leunig, M.; Jain, R. K. Fluorescence photobleaching with spatial Fourier analysis: measurement of diffusion in light-scattering media. *Biophys. J.* **1993**, *65*, 2428−2436.
(26) Tsay, T. T.; Jacobson, K. A. Spatial Fourier analysis of video photobleaching measurements. *Biophys. J.* **1991**, *60*, 360−368.
(27) Jönsson, P.; Jonsson, M. P.; Tegenfeldt, J. O.; Höök, F. A Method Improving the Accuracy of Fluorescence Recovery after Photobleaching Analysis. *Biophys. J.* **2008**, *95*, 5334−5348.
(28) Richbourg, N. R.; Wancura, M.; Gilchrist, A. E.; Toubbeh, S.; Harley, B. A. C.; Cosgriff-Hernandez, E.; Peppas, N. A. Precise control of synthetic hydrogel network structure via linear, independent synthesis-swelling relationships. *Sci. Adv.* **2021**, *7*, eabe3245.
(29) Armstrong, J. K.; Wenby, R. B.; Meiselman, H. J.; Fisher, T. C. The Hydrodynamic Radii of Macromolecules and Their Effect on Red Blood Cell Aggregation. *Biophys. J.* **2004**, *87*, 4259−4270.
(30) Casalini, T.; Salvalaglio, M.; Perale, G.; Masi, M.; Cavallotti, C. Diffusion and Aggregation of Sodium Fluorescein in Aqueous Solutions. *J. Phys. Chem. B* **2011**, *115*, 12896−12904.
(31) Favre, E.; Leonard, M.; Laurent, A.; Dellacherie, E. Diffusion of polyethyleneglycols in calcium alginate hydrogels. *Colloids Surf., A* **2001**, *194*, 197−206.
(32) Li, X.; Sakai, T. Mass Transport in Polymer Gels. *Phys. Polym. Gels* **2020**, 137−150.
(33) Fathi, E.; Atyabi, N.; Imani, M.; Alinejad, Z. Physically crosslinked polyvinyl alcohol−dextran blend xerogels: Morphology and thermal behavior. *Carbohydr. Polym.* **2011**, *84*, 145−152.
(34) Liu, P.; Chen, W.; Liu, C.; Tian, M.; Liu, P. A novel poly (vinyl alcohol)/poly (ethylene glycol) scaffold for tissue engineering with a unique bimodal open-celled structure fabricated using supercritical fluid foaming. *Sci. Rep.* **2019**, *9*, 9534.
(35) Pluen, A.; Netti, P. A.; Jain, R. K.; Berk, D. A. Diffusion of Macromolecules in Agarose Gels: Comparison of Linear and Globular Configurations. *Biophys. J.* **1999**, *77*, 542−552.
(36) Lee, H.; Venable, R. M.; MacKerell, A. D., Jr.; Pastor, R. W. Molecular Dynamics Studies of Polyethylene Oxide and Polyethylene Glycol: Hydrodynamic Radius and Shape Anisotropy. *Biophys. J.* **2008**, *95*, 1590−1599.
(37) Venturoli, D.; Rippe, B. Ficoll and dextran vs. globular proteins as probes for testing glomerular permselectivity: effects of molecular size, shape, charge, and deformability. *Am. J. Physiol.* **2005**, *288*, F605−F613.
(38) Amsden, B. Solute Diffusion within Hydrogels. Mechanisms and Models. *Macromolecules* **1998**, *31*, 8382−8395.
(39) Parrish, E.; Rose, K. A.; Cargnello, M.; Murray, C. B.; Lee, D.; Composto, R. J. Nanoparticle diffusion during gelation of tetra poly(ethylene glycol) provides insight into nanoscale structural evolution. *Soft Matter* **2020**, *16*, 2256−2265.
(40) Rose, K. A.; Molaei, M.; Boyle, M. J.; Lee, D.; Crocker, J. C.; Composto, R. J. Particle tracking of nanoparticles in soft matter. *J. Appl. Phys.* **2020**, *127*, 191101.

https://doi.org/10.1021/acs.macromol.1c01752
Macromolecules 2021, 54, 10477−10486